UvA-DARE (Digital Academic Repository)

Cosmological searches for a noncold dark matter component

Gariazzo, S.; Escudero, M.; Diamanti, R.; Mena, O.

Link to publication

Cosmological searches for a noncold dark matter component

Stefano Gariazzo,[1] Miguel Escudero,[1] Roberta Diamanti,[2] and Olga Mena[1]

[1]*Instituto de Física Corpuscular (IFIC), CSIC-Universitat de Valencia,*
Apartado de Correos 22085, E-46071, Spain
[2]*GRAPPA Institute of Physics, University of Amsterdam,*
Science Park 904, 1098 GL Amsterdam, Netherlands

We explore an extended cosmological scenario where the dark matter is an admixture of cold and additional noncold species. The mass and temperature of the noncold dark matter particles are extracted from a number of cosmological measurements. Among others, we consider tomographic weak lensing data and Milky Way dwarf satellite galaxy counts. We also study the potential of these scenarios in alleviating the existing tensions between local measurements and cosmic microwave background (CMB) estimates of the S_8 parameter, with $S_8 = \sigma_8 \sqrt{\Omega_m}$, and of the Hubble constant H_0. In principle, a subdominant, noncold dark matter particle with a mass $m_X \sim$ keV, could achieve the goals above. However, the preferred ranges for its temperature and its mass are different when extracted from weak lensing observations and from Milky Way dwarf satellite galaxy counts, since these two measurements require suppressions of the matter power spectrum at different scales. Therefore, solving simultaneously the CMB-weak lensing tensions and the small scale crisis in the standard cold dark matter picture via only one noncold dark matter component seems to be challenging.

I. INTRODUCTION

Within the current canonical cosmological model, dubbed the ΛCDM model, the dark matter is assumed to be made of a totally cold gas of weakly interacting particles, accounting for $\sim 26\%$ of the current Universe mass-energy density. This standard picture has been extremely successful in explaining both the large scale structure observations of our Universe and the pattern of the temperature and polarization fluctuations in the cosmic microwave background (CMB) [1]. Nevertheless, the mechanism explaining the origin and the physics of this cold dark matter component remains obscure [2–4], with possible candidates ranging from the GeV–TeV energy scale to very light (μeV) dark matter axions. Together with this hitherto theoretically unknown cold dark matter nature, there are a number of observations which further motivate the searches for other possible dark matter candidates.

On the one hand, there is the *small scale crisis* of the ΛCDM model. This problem is closely related to several galactic and subgalactic phenomena, as the *Milky Way satellites problem* [5,6] and the so-called *too big to fail problem* [7], which refer to the fact that the predictions from the ΛCDM picture fail in reproducing the number of low-mass subhalos expected within a Milky Way-sized halo and the measured kinematics of the Milky Way satellites, respectively. A large effort in the literature has been devoted to alleviate these problems [8–19].

On the other hand, recent measurements of tomographic weak gravitational lensing, as those from the Kilo Degree-450 deg^2 Survey (KiDS-450) [20,21], show substantial discordances with CMB measurements from Planck [1,22]

in the matter perturbations at small scales. These discordances are quantified in terms of the extracted values of the amplitude of the small-scale density fluctuations, quantified by the parameter σ_8, at a given matter density, Ω_m. In particular, the quantity $S_8 = \sigma_8 \sqrt{\Omega_m}$ as measured by KiDS is in tension with the Planck estimate at the level of 2.3σ [20]. Similar results had already appeared in the past from the analyses of CFHTLenS data [23,24]. A number of recent dedicated studies in the literature have shown that the CFHTLenS and the KiDS discrepancies are independent of the small-angle approximations commonly exploited in weak lensing data analyses [25–27].

Here, instead of refining cosmic shear analyses, we follow a different avenue to ameliorate these problems. In the spirit of Ref. [21], we consider a modified version of the most economical pure cold dark matter model, allowing for a mixed dark matter cosmology with an additional, nontotally cold, dark matter relic. These models with an admixture of cold and noncold dark matter particles have been dubbed mixed dark matter (MDM) models; see e.g. Refs. [28–33]. The motivation to consider these models is twofold: in addition to their potential in alleviating the tension between cosmic-shear and CMB measurements, they could also provide a solution to the aforementioned ΛCDM small-scale crisis, while leaving unchanged the predictions from the ΛCDM model at large scales. The reason is simple: the particle associated to the second, nontotally cold dark matter component will have a significant free-streaming length, that affects the matter power spectrum on the smallest scales, therefore improving the compatibility with the observations of the local Universe [34] through a reduction of the S_8 quantity.

043501-1

In this study we scrutinize these mixed dark matter scenarios, using the most recent tomographic weak lensing measurements from the KiDS-450 survey, in combination with Planck CMB data. By means of these data sets we shall derive constraints on the current temperature and mass-energy density of the noncold dark matter component, searching for the most favored cosmological dark matter scenario. Furthermore, we also consider current estimates from the observed number of Milky Way satellite galaxies, comparing these results to those preferred by weak lensing data.

The structure of the paper is as follows. In Sec. II we present the methodology followed here, describing the mixed dark matter model, the included data sets and the technical details of our numerical analyses. Our results are shown in Sec. III. We draw our main conclusions in Sec. IV.

II. METHODOLOGY

A. Mixed dark matter modeling

In this paper we explore a scenario where the dark matter fluid is made of two components: one which corresponds to the standard cold dark matter (CDM) plus a second one with a nonzero temperature T_X, which is a warm dark matter (WDM) component.[1] In the following we shall refer to this model as the mixed dark matter (MDM) model. While the CDM component is simply parametrized via its energy density $\omega_c \equiv \Omega_c h^2$, the second dark matter component is parametrized through its temperature T_X and its energy density fraction f_X relative to the total dark matter component $\omega_{DM} = \omega_X + \omega_c$, defined as

$$f_X = \frac{\omega_X}{\omega_{DM}}, \tag{1}$$

where $\omega_i \equiv \Omega_i h^2$ refers to the present mass-energy density. Notice that the mass of the second, noncold dark matter particle can be computed from its energy density and its temperature using the relation

$$\omega_X = \left(\frac{T_X}{T_\nu}\right)^3 \left(\frac{m_X}{94 \text{ eV}}\right). \tag{2}$$

In our analyses we shall consider $0 \leq f_X \leq 1$ for the WDM energy density and $-1.5 \leq \log_{10}(T_X/T_\nu) \leq 0$ for its temperature. The upper temperature prior, $T_X = T_\nu$, is fixed to be the one corresponding to the pure *hot* dark matter regime, i.e. to the standard neutrino temperature, while the lower prior is chosen in order to preserve the validity of the numerical calculations for the MDM model used here, as we explain in what follows.

A crucial point when dealing with the MDM modeling is related to the power spectrum of the density perturbations, which is modified when a second nontotally cold dark matter component is also considered in the cosmological evolution. The deviations of the matter power spectrum in the MDM model from its standard shape within the CDM model may be highly nontrivial and must be treated cautiously, since we are dealing with weak lensing probes, which require a good knowledge of the perturbation behavior in the nonlinear regime.[2] We recall that the nonlinear approximations that are commonly used for the numerical computations are calibrated on N-body simulations. These calibrations, however, must be considered carefully, since the extrapolation for unusual models may spoil the correctness of the adopted formulas.

In this regard, we show in Fig. 1 the relative difference between the nonlinear matter power spectrum of some of the MDM models explored here with respect to the corresponding CDM only case. We use $\omega_{DM} = 0.12$ for all the plots, with $f_X = 0$ for the CDM-only model and $f_X = 0.5$ for the other cases, and we vary the noncold dark matter particle temperature. The panels refer to four possible nonlinear prescriptions: the standard [36–39] (upper left panel) and the accurate [40] (upper right panel) versions of the halo model, the standard `halofit` code [41] (lower left panel) and the fitting formula presented in Ref. [42] (lower right panel), that we shall adopt here (see below). Notice that the `halofit` prescription badly fails in reproducing the expected behavior of the nonlinear power spectrum when the temperature T_X of the nontotally cold dark matter particle deviates significantly from the neutrino temperature, T_ν. In the limit $T_X \to 0$, the MDM case should approach the CDM one, eventually overlapping with it, and this behavior is clearly not reproduced. The accurate halo model[3] also presents some problems at the smallest scales. Following these results, the best model to describe the nonlinear perturbation growth in the MDM case seems to be the standard halo model. However, even in this case there exists an unphysical bump at scales $k \sim 1~h/\text{Mpc}$ which makes its predictions unreliable.

The clear failure of these three widely used nonlinear models for a significant range of temperatures T_X has motivated us to search for an alternative description of the nonlinearities in the power spectrum in the presence of an additional noncold dark matter component. We have therefore adopted the prescriptions presented in Ref. [42], that we briefly summarize here.

Starting from the standard nonlinear matter power spectrum for a CDM universe P_{CDM} computed with {[41,43], the

---

[1]We consider relics with a Fermi-Dirac distribution. A change in the distribution will not change dramatically the results, see e.g. [33].

[2]This is a delicate issue, as we are dealing with a second dark matter component different from the standard three neutrino active contribution. For the implementation of massive neutrinos in nonlinear matter power spectrum simulations, see Ref. [35].

[3]The term "accurate" is related to the fact that this improved version of the original halo model [36–39] takes into account several corrections (that include, among others, the baryonic feedback), i.e. factors that are not included in the standard halo model, see Ref. [40] for details.
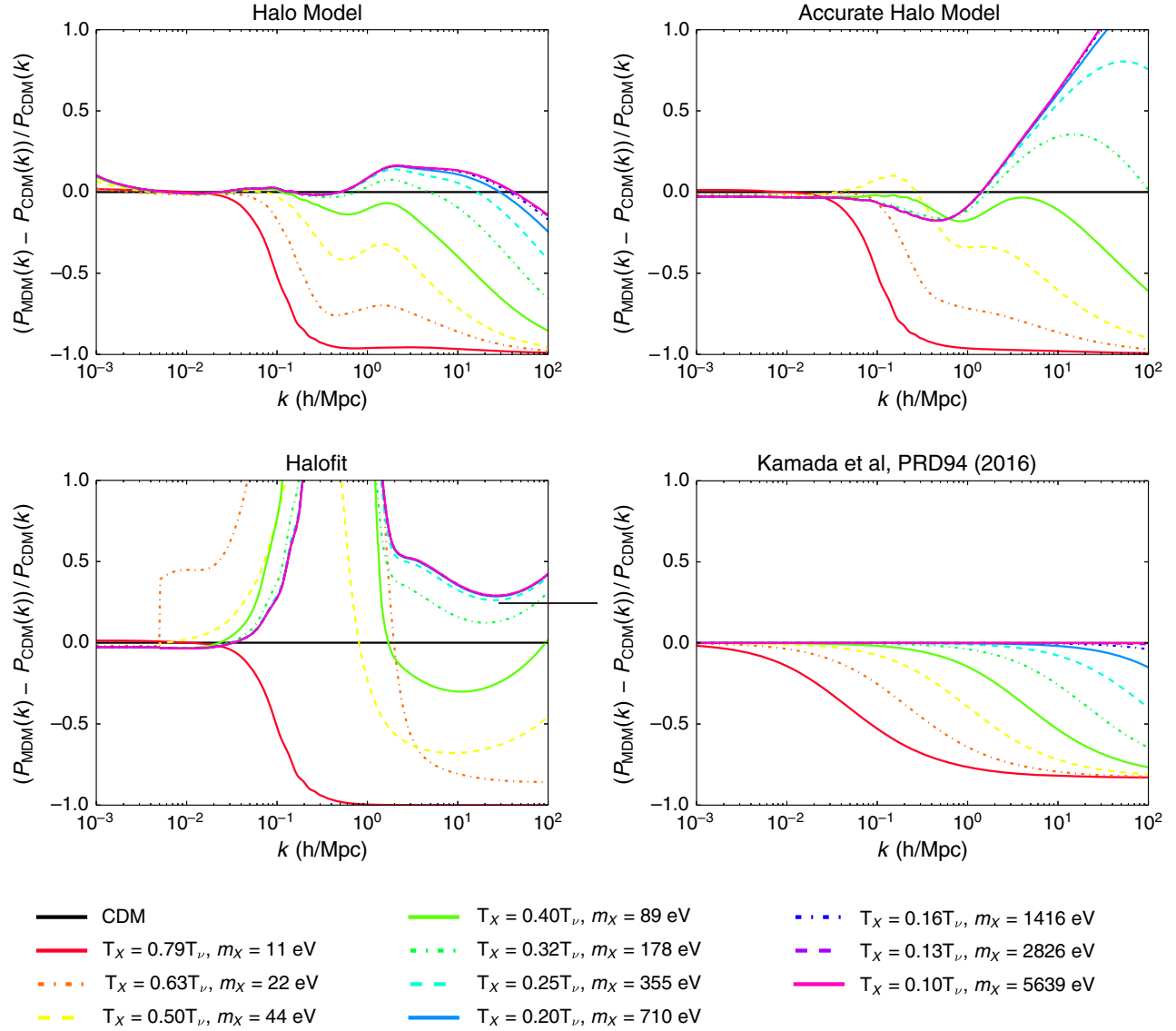
FIG. 1. Relative difference of the MDM nonlinear matter power spectrum at $z = 0$ (for $f_X = 0.5$) with different temperatures T_X, with respect to the pure CDM case (for which $f_X = 0$), for four different nonlinear approaches, as described in the text. For all of them we fix $\omega_{DM} = 0.12$. The nonlinear prescription adopted in this work, given by Ref. [42], is the one corresponding to the *lower right* panel.

authors of Ref. [42] find that the fitting function that best matches the results of N-body simulations in the presence of a noncold dark matter component is given by

$$\frac{P_{\mathrm{MDM}}(k)}{P_{\mathrm{CDM}}(k)} = T^2(k; r_X, k'_d)$$

$$= (1 - r_X) + \frac{r_X}{(1 + k/k'_d)^{0.7441}}, \quad (3)$$

where the two quantities that appear in the right-hand side read as

$$r_X(f_X) = 1 - \exp\left(-a\frac{f_X^b}{1 - f_X^c}\right), \quad (4)$$

$$k'_d(k_d, f_X) = k_d \cdot f_X^{-5/6}. \quad (5)$$

In the latter equation, k_d is the damping scale given in Ref. [44] as a function of the linear growth rate $D(z)$,

$$k_d(m_X, z) = \left(\frac{m_X}{\mathrm{keV}}\right)^{2.207} D(z)^{1.583} 388.8 \, h \, \mathrm{Mpc}^{-1}. \quad (6)$$

Finally, parameters a, b, c in Eq. (4) are obtained by fitting the parametrization above to the N-body simulation results [42],

$$a = 1.551, \qquad b = 0.5761, \qquad c = 1.263. \quad (7)$$

In all the relevant parts of our computation, therefore, we substituted the nonlinear matter power spectrum with the one given by Eq. (3). This means that we need

to compute the nonlinear matter power spectrum P_{CDM} in the CDM-only model using the standard HALOFIT prescription.

B. Data sets

1. Cosmic microwave background (CMB)

We consider the CMB measurements of the most recent Planck data release [1,22], using the full temperature power spectrum at all multipoles ($2 \leq \ell \leq 2500$, Planck TT), the polarization power spectra only in the low multipoles range ($2 \leq \ell \leq 29$, lowP) and the lensing likelihood computed from the 4-point correlation function. Since there could be still some level of residual systematics contamination [1], we neglect the polarization measurements at high multipoles (highP), following therefore a very conservative approach which will ensure very robust limits. We refer to the Planck TT + lowP + lensing combination of data as the "CMB" data set.

2. KiDS data

An essential point of this study is the addition of the measurements of the Kilo Degree Survey (KiDS) [20,21] using the methodology explained in [20].

The KiDS data can be used to reconstruct the 2-point shear correlation functions $\xi_\pm^{ij}(\theta)$ for the i, j tomographic bin combination at the angle θ. The data set that we use here is from KiDS-450 [20,45,46] and covers an effective area of 360 deg^2. The median redshift is $z_m = 0.53$, while the effective number density is $n_{eff} = 8.5$ galaxies arcmin^{-2}. The experiment covers 7 angular bins in the range 0.5 to 72 arcmins for $\xi_+^{ij}(\theta)$ and 6 angular bins between 4.2 and 300 arcmins for $\xi_-^{ij}(\theta)$.

The calibration of the photometric redshift distributions is made through the "weighted direct calibration" (DIR) method presented in Ref. [20]. This uses the data of external, overlapping spectroscopic surveys and creates series of 1000 bootstrap realizations to obtain the uncertainties and the correlations between the tomographic bins. Each bootstrap sample is used for a fixed number of iterations of the MCMC scan performed here. This bootstrap procedure ensures that the analysis is statistically unaffected by the photometric redshift bias corrections [21], which can instead significantly change the results of the analysis of e.g. CFHTLenS data and may alleviate the tension with the value of σ_8 determined by Planck [47].

Furthermore, the KiDS data are analyzed taking into account the intrinsic galaxy alignments, for which the correlations of intrinsic ellipticities of galaxies with each other and with the shear of background sources must be considered. This is done varying two nuisance parameters: the amplitude A_{IA} and the redshift dependence η_{IA} (see Ref. [48]). As we have checked that our results do not change significantly if we turn on these "extended systematics"

settings [21], we will only show the results obtained within the standard prescription, i.e. $\eta_{IA} = 0$ and $-6 \leq A_{IA} \leq 6$.

To perform the analyses as presented by the KiDS Collaboration [20,21], we should include the calculation of baryonic effects in the nonlinear matter power spectrum, that are computed using HMCODE [40]. As we discussed in Sec. II A, this code gives biased results when applied to the (unusual) MDM cosmology when the noncold dark matter temperature is much smaller than the standard neutrino one. Since we are using Eq. (3) for computing the nonlinear matter power spectrum, we shall not use HMCODE and the related prescriptions on the baryonic feedback.

3. Satellite galaxies

As we have already introduced, one of the problems of the ΛCDM model at galactic and subgalactic scales is the one of the missing satellite galaxies. Here we explain how we compute the constraints from the observations of dwarf satellite galaxies in the Milky Way (MW).

Dwarf galaxies are usually faint and small objects that must be observed and correctly identified as satellites of the MW. In the following we briefly comment on the current observational status [49,50]. The number of known standard satellites of our Galaxy is eleven. The SDSS experiment, with a sky coverage of $f_{sky} \simeq 0.28$, observed other fifteen satellites [51], with a corresponding Poissonian error of ∼4. Recently, the Dark Energy Survey (DES) has reported the discovery of eight new Milky Way companions, which could potentially be ultrafaint satellite galaxies [52,53]. In the absence of a robust confirmation of the fact that these new eight DES candidates are truly all of them Milky-Way satellite galaxies, we adopt here the conservative approach of Ref. [49] and restrict ourselves to the classical satellites plus the extrapolated number of the SDSS measurements, see the discussion that follows.

We assume here that the number within the SDSS footprint is binomially distributed with probability $f_{sky} \simeq 0.28$, following an isotropic distribution. Then, a SDSS-like experiment would have observed 54 MW satellite galaxies over the entire sky, with an associated (binomial distribution) error of 11. Therefore, together with the eleven classical MW satellites, this would imply a total number of $N_{sat} = 65 \pm 11$. Following Ref. [49], we assume a halo-to-halo scatter [54] by reducing our estimated number of MW satellite galaxies, quoted above, by 10%. Nevertheless, we are aware that this number is probably an underestimate of the true number of dwarf satellites, as a consequence of the technical challenges of the observation. Notice however that, due to the incompleteness of the SDSS sample, it could be possible that, when accounting for corrections in e.g. the observed luminosity function, the number of satellite galaxies around the MW could be much larger than these estimates, see e.g. Ref. [55]. For this reason, we present the results obtained combining the satellites likelihood with other data sets following two different approaches. In the most conservative scenario,

labeled "SAT(low)" in the following, we apply the observed number of MW dwarf satellite galaxies $N_{\text{sat}}^{\text{obs}} = 58 \pm 11$ as a lower limit only, by means of a half-Gaussian likelihood, following e.g. Ref. [33]. In this conservative approach we apply the dwarf galaxy bounds only when the number of satellite galaxies predicted within a given model is below the mean number of satellite galaxies that are observed. In this way we envisage the putative situation in which not all dwarf spheroidal galaxies have been detected, being the current estimates subject to increase by ongoing and/or future searches. We also follow a more aggressive scenario in which we apply the current measurement $N_{\text{sat}}^{\text{obs}} = 58 \pm 11$ via a standard Gaussian likelihood. This latter case will be referred to as "SAT".

Another problem related to dwarf satellites is that it is also difficult to infer the mass of these objects, since they are dominated by dark matter, and the only possibility to measure the properties of the DM halo is through stellar kinematics inside the object. Studies that use different profiles for the halo suggest that all the known dwarfs have a mass larger than $M_{\text{min}} = 10^8 h^{-1} M_\odot$ [56], a number that we shall use in the calculations explained below.

For the theoretical computation of the number of satellites we follow the procedure described in Refs. [33,49,57], based on a conditional mass function that is normalized taking into account the results of the N-body simulations. The function which gives the expected number of dwarf satellite galaxies with a given mass M_s reads as [49,57]

$$\frac{dN_{\text{sat}}}{d \ln M_s} = \frac{1}{C_n} \frac{1}{6\pi^2} \left(\frac{M_h}{M_s} \right) \frac{P(1/R_s)}{R_s^3 \sqrt{2\pi(S_s - S_h)}}. \quad (8)$$

Here $P(1/R_s = k)$ is the linear matter power spectrum for the given cosmological model, h stands for "host halo", i.e. the MW galaxy, and the subscript s stands for "satellite" or "subhalo". The coefficient $C_n = 45$ is chosen to mimic the results of N-body simulations [17]. In our calculations we assume $M_h = 1.77 \times 10^{12} h^{-1} M_\odot$ for the MW. This may be not the exact mass of our Galaxy, but it is chosen because it lies in the estimated range for the MW mass [58], and it matches the mass of the Aquarius-D2 simulation [59], from which the calibration on the N-body simulations results is computed [17]. The estimated number of satellites $N_{\text{sat}}^{\text{th}}$ is obtained integrating the above Eq. (8) between the minimum mass of satellites M_{min}, previously described, and the mass of the host halo M_h,

$$N_{\text{sat}}^{\text{th}} = \int_{M_{\text{min}}}^{M_h} \frac{dN_{\text{sat}}}{d \ln M_s} dM_s. \quad (9)$$

The parameters describing the subhalo (or the host halo) are the radius R_s (R_h), the mass M_s (M_h) and the corresponding variance S_s (S_h). They are related by

$$S_i(M) = \frac{1}{2\pi^2} \int_0^\infty k^2 P(k) W^2(k|M) dk, \quad (10)$$

$$M_i = \frac{4\pi}{3} \Omega_m \rho_c (cR_i)^3, \quad (11)$$

where $i = s, h$. The parameter $c = 2.5$ is used to calibrate the calculation on N-body simulation results.

To evaluate the variance, we use a procedure based on a rederivation of the Press and Schechter [60] mass function, for which we use a *k-sharp filter* approach [18] to cut all the scales k below the cutoff scale $k_s = 1/R_s$, and R_s depends on the subhalo mass as in Eq. (11). This filter is written in terms of a window function

$$W(k|M) = \begin{cases} 1, & \text{if } k \le k_s(M); \\ 0, & \text{if } k > k_s(M). \end{cases} \quad (12)$$

C. Numerical analyses

We base our analyses on the standard ΛCDM model, with the addition of a second noncold dark matter component. The parameters that we vary in our analyses are then the energy density of baryons, $\omega_b \equiv \Omega_b h^2$; the total energy density of the dark matter components ω_{DM}, the fraction of the total dark matter mass-energy density in the form of noncold dark matter (f_X) and its temperature through the logarithm $\log_{10}(T_X/T_\nu)$ (see also Sec. II A); the optical depth to reionization, τ; the ratio of the sound horizon to the angular diameter distance at decoupling Θ; and the amplitude and the tilt of the primordial power spectrum of curvature perturbations, $\ln(10^{10} A_s)$ and n_s.

Other cosmological parameters are fixed to their standard values as follows. The sum of the three active neutrino masses is fixed to zero. Despite neutrino oscillation measurements tell us that at least two of the neutrinos must have a mass, with a minimum total mass of $\sum m_\nu \simeq 0.06$ eV for the normal ordering, the error that we make when fixing $\sum m_\nu \simeq 0$ is small. For the three massless neutrinos, we fix the standard value $N_{\text{eff}}^\nu = 3.046$, corresponding to the three active neutrino contribution obtained in the limit of noninstantaneous neutrino decoupling [61,62].

For the Planck CMB and satellite galaxy number counts we use the Markov chain Monte Carlo (MCMC) tool Monte Python [63], interfaced with the Boltzmann solver CLASS [64]. We use then the obtained covariance matrices to run MCMC with KiDS data, by means of the Boltzmann solver CAMB [65] together with its MCMC companion CosmoMC [66].[4]

---

[4]For the latter one, we use the July 2015 version with the required modifications to perform the analyses of the KiDS data [21], publicly available at http://github.com/sjoudaki/kids450.

Together with the cosmological parameters, we vary all the required nuisance parameters involved in the Planck and the KiDS likelihoods.

III. RESULTS

Figure 2, left panel, depicts the 68% and 95% C.L. allowed contours in the (Ω_m, σ_8) plane resulting from a number of possible data combinations and comparing different underlying cosmological models. In the simplest ΛCDM picture, the allowed regions for the KiDS and Planck data sets do not basically overlap, showing a clear tension, as pointed out before by Refs. [20,21]. Such a tension is clearly alleviated when one considers the possible MDM extension to the minimal ΛCDM picture: notice that the contours for KiDS and Planck overlap for a larger region in the MDM case. This very same improvement can be noticed from the one-dimensional posterior probability distribution of the $S_8 = \sigma_8\sqrt{\Omega_m}$ quantity in the right panel of Fig. 2.

A possible way of quantifying the tension in the measurements of S_8 arising from the Planck and KiDS data sets in possible extensions of the ΛCDM framework has been presented and used in Ref. [21]. The tension is defined by

$$T(S_8) \equiv |\bar{S}_8^{D_1} - \bar{S}_8^{D_2}|/\sqrt{\sigma^2(S_8^{D_1}) + \sigma^2(S_8^{D_2})}, \quad (13)$$

where D_1 and D_2 refer to the Planck and KiDS data sets, $\bar{S}_8$ is the mean value over the posterior distribution and σ refers to the 68% C.L. error on S_8. If we compute the value of $T(S_8)$ from the constraints obtained within the MDM scenario explored here, we get a displacement of $T^{\mathrm{MDM}}(S_8) \simeq 1\sigma$, which indicates that the 2.3σ–2.8σ[5] obtained between Planck and KiDS S_8 values within the canonical ΛCDM scenario is considerably reduced. The level of the improvement is very similar to that reached when other possible extensions to the minimal scenario are considered, as, for instance, in the presence of a dark energy equation of state or within modified gravity models [21]. The fact that assuming a MDM scenario the tension between the Planck and KiDS constraints is strongly alleviated fully justifies the combination of these two data sets, already depicted in both panels of Fig. 2.

Figure 3 shows the two-dimensional 68% and 95% C.L. allowed contours in the (S_8, T_X/T_ν) and (S_8, f_X) planes. We illustrate the results from KiDS, CMB and their combination. We can notice from the contours shown in

---

[5]The authors of [20] quote a 2.3σ tension among the obtained S_8 values from Planck (CMB temperature and low-ℓ polarization) and KiDS. Our analysis of the KiDS results with the prescriptions published together with Ref. [21] leads to a value of $T(S_8) \simeq 2.8$, with small variations when we consider our results from Planck CMB data or the Planck chains publicly available at https://wiki.cosmos.esa.int/planckpla. When the full CMB data set we explore here is considered, which includes the Planck lensing likelihood, the tension shifts to $T(S_8) \simeq 2.5$.

the left panel of Fig. 3 that there exists a degeneracy between the S_8 quantity and T_X/T_ν. The reason for that is because the larger T_X is, the closer the noncold dark matter component behaves as a hot dark matter fluid, and therefore a larger matter component (and, consequently, a larger value of S_8) would be required to compensate for the suppression of perturbations at small scales. As expected, there are no bounds on the noncold dark matter fraction f_X, as one can see in the right panel of Fig. 3. Indeed, for a very small value of T_X the noncold dark matter is observationally indistinguishable from a pure cold component, and therefore its relative abundance is perfectly compatible with $f_X = 1$.

As previously stated, the motivation for MDM scenarios is twofold. We have already shown above that a noncold dark matter component provides a possible way of alleviating the tension between Planck CMB measurements and tomographic weak lensing data from KiDS. As mentioned in our introductory section, there is another very important motivation to look for additional extensions of the minimal cold dark matter picture, namely, the so-called small scale crisis of the ΛCDM, and, in particular, the *Milky Way satellite problem* [5,6]. We have therefore also considered in our analyses the constraints from the MW dwarf satellite galaxies, that we are going to discuss in what follows.

The first panel of Fig. 4 shows the one-dimensional probability distribution of the noncold dark matter temperature relative to that of the neutrino bath T_X/T_ν. Planck CMB data measurements provide the 95% C.L. upper bound of $T_X/T_\nu < 0.4$, which could be naively translated into a contribution to $\Delta N_{\mathrm{eff}} = (T_X/T_\nu)^4 \simeq 0.02$ during the periods in the Universe expansion history in which these noncold dark matter particles are relativistic. Notice that this value is much smaller than the limit obtained from Planck CMB measurements on the contribution from (massless) dark radiation or light sterile neutrinos. However, the limits are not directly comparable as the energy density of the noncold dark matter component explored here is that of a nonrelativistic fluid for a large region of the parameter space. KiDS measurements show a preference for higher temperatures, indeed the 95% C.L. upper limit is set by the upper prior in the T_X/T_ν ($T_X/T_\nu < 1$) parameter. When analyzing KiDS data taking into account the Planck CMB constraints on all the cosmological parameters, we obtain $T_X/T_\nu < 0.6$ at 95% C.L. We also show in Fig. 4 the results obtained combining the MW satellites counts with CMB measurements. The blue curve depicts the one-dimensional probability distribution of the noncold dark matter temperature when the current estimates of MW satellite galaxies are treated as regular Gaussian priors and are combined with Planck CMB measurements. This data combination constrains the temperature to lie within a narrow region, favoring scenarios with values of T_X/T_ν in the range $0.15 < T_X/T_\nu < 0.17$, therefore smaller than those quoted
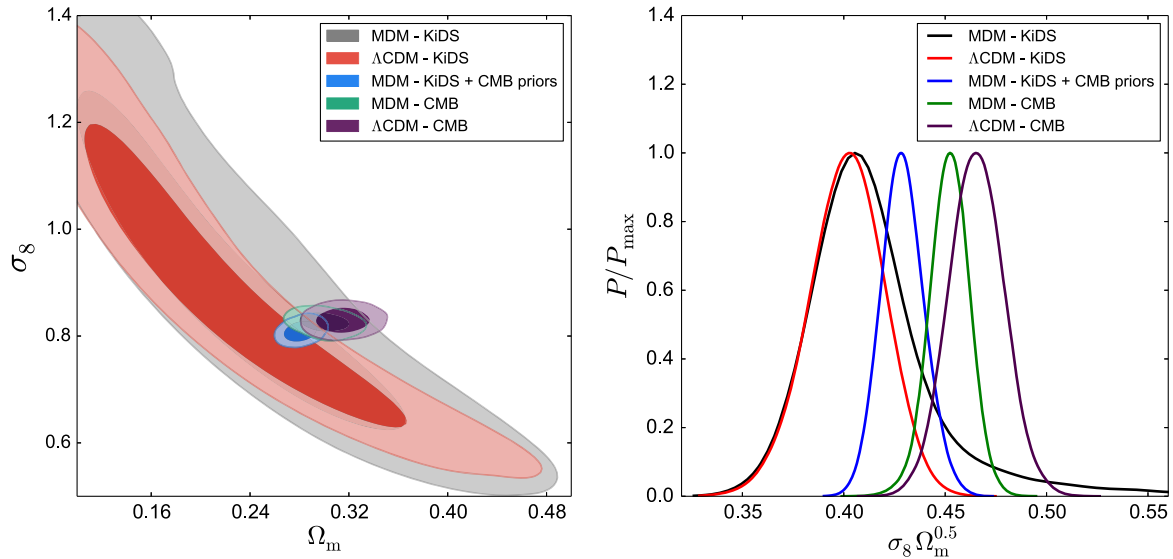
FIG. 2.   Left panel: 68% and 95% C.L. allowed contours in the (Ω_m, σ_8) plane, see text for details. Right panel: one-dimensional posterior probability distribution of the S_8 quantity for the same data combinations and models shown in the left panel.
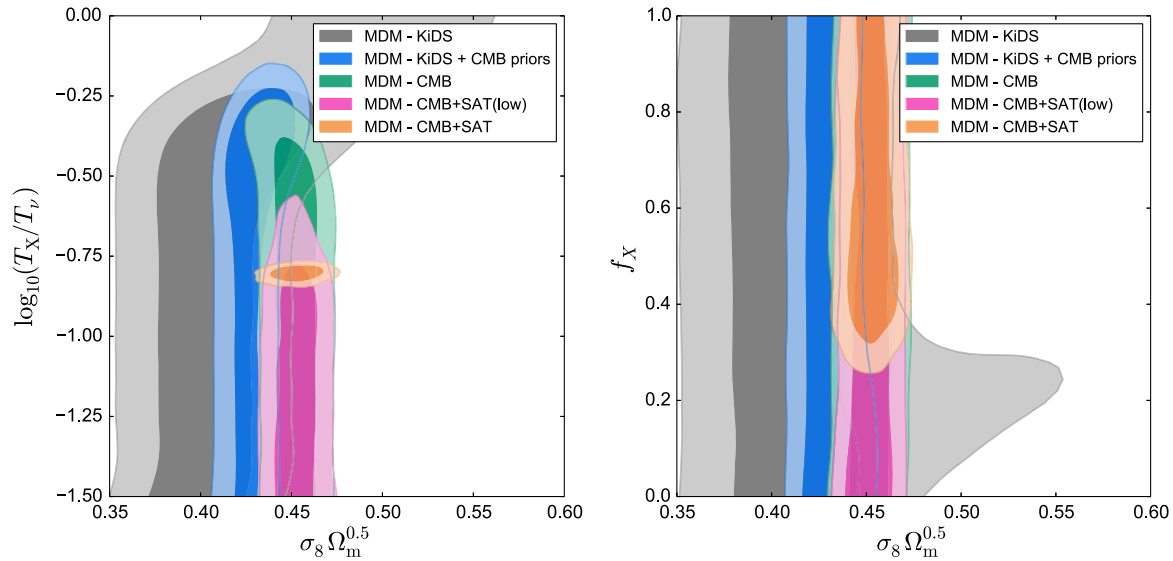

FIG. 3.   68% and 95% C.L. allowed contours in the $(S_8, T_X/T_\nu)$ and (S_8, f_X) planes resulting from different data sets: KiDS alone, CMB alone, the combination of KiDS and CMB data, and the combination of CMB measurements with MW satellite number counts, see text for details.

previously for the KiDS plus Planck MDM case. This difference can be explained in terms of the preferred value of m_X, which turns out to be larger for Planck plus MW satellites than for Planck plus KiDS data. If we instead consider the MW likelihood in the form of a conservative half-Gaussian likelihood, imposing the current observed number of galaxies only as a lower limit, there is no lower bound on the noncold dark matter temperature, as the half-Gaussian likelihood turns out to be perfectly compatible with a pure ΛCDM universe, for which the number of satellite galaxies is around 160. The upper limit on T_X/T_ν is very close to the one quoted above for our more

aggressive MW likelihood scenario ($T_X/T_\nu < 0.19$ at 95% C.L.), and smaller also than the constraint obtained from Planck plus KiDS data.

The second panel of Fig. 4 shows the one-dimensional probability distribution of the noncold dark matter mass m_X.[6] Notice that there exist a 95% C.L. lower limit from Planck data on the mass of the MDM component $m_X > 32$ eV. This bound on the mass is related to the fact that, below that region, the noncold dark matter fluid

---

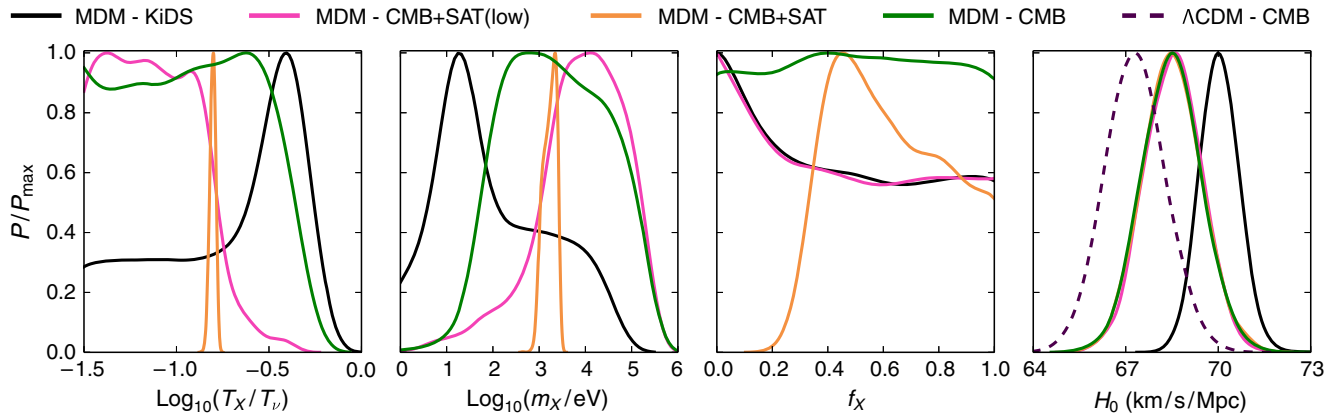[6]We recall that m_X is a derived parameter in our analyses.

FIG. 4.   One-dimensional posterior probability distribution for the T_X/T_ν ratio, for the noncold dark matter mass m_X, its relative fraction f_X and for the Hubble constant H_0 for different data combinations in the MDM scenario, see the text for details. For comparison purposes, in the case of the Hubble constant, we also depict the resulting one-dimensional distribution from a fit to Planck CMB data in the context of a ΛCDM cosmology.

behaves as a *hot* dark matter component (even if its temperature is lower than the neutrino one), and CMB observations do not allow for such large contribution from hot dark matter relics. On the other hand, KiDS measurements show a mild preference for a dark matter mass in the sub-keV region, that can provide the suppression of the small-scale perturbations required to reduce the value of the S_8 quantity for KiDS. The combination of Planck CMB plus KiDS weak lensing data does not significantly change these findings.

When considering the MW dwarf satellite constraints in their less conservative form, we observe that there is a preferred narrow region for the noncold dark matter mass, which, as we shall further illustrate in short, turns out to be very close to the warm dark matter region[7] The mass of the particle lies in the range 0.95 keV $< m_X <$ 2.9 keV (95% C.L.). Additional and independent constraints from power spectrum measurements from the Lyman alpha forest flux and from the universe reionization history can be applied in this case, see Refs. [72–76] for the most recent analyses.

When adopting the more conservative, half-Gaussian approach for the MW likelihood, the lower bound we get for the noncold dark component is very close to the region quoted above, $m_X >$ 0.09 keV at 95% C.L., as lower values of the noncold dark matter mass will lead to a very large suppression of the matter power spectrum at galactic and subgalactic scales, in which case the number of MW satellite galaxies gets strongly reduced. However, for this case, there is no upper limit on m_X, as a model with only the cold dark matter component is perfectly allowed once the upper bound in the observed number of MW galaxies is no longer considered, largely relaxing the allowed mass range.

Notice that the preferred region for the mass m_X obtained considering the MW satellites observations is larger than the one suggested by KiDS weak lensing measurements. This is due to the fact that the suppression in the growth of structure required to satisfy MW satellite galaxy observations is associated to a smaller scale (large wave number k) than the one required to explain KiDS weak lensing data. The differences in the preferred values of m_X from weak lensing and from KiDS lead to differences in the allowed values of T_X/T_ν. As previously stated, the bound on m_X directly depends on the constraint in the abundance of the particle. Consequently, the larger (smaller) the allowed mass is, the smaller (larger) the temperature should be to satisfy CMB constraints, see Eq. (2).

The bounds on the noncold dark matter fraction are shown in the third panel of Fig. 4. Planck measurements result in an almost completely flat distribution for f_X, as particles with small temperatures and large masses will produce CMB photon temperature and lensing patterns that are identical to those obtained in the pure cold dark matter case. KiDS and its combination with CMB measurements lead also to flat distributions for f_X, with limits coinciding with the assumed priors on f_X. When dealing with the MW satellites likelihood in the less conservative approach, its combination with Planck CMB sets a robust preference for $f_X > 0$, i.e. $f_X >$ 0.34 at 95% C.L., while in the more conservative approach the f_X distribution is flat. Therefore, the results that we obtain when considering the MW dwarf satellites in the less conservative approach followed here strongly suggest the need for a nonzero noncold dark matter component. The explanation is simple: while we observe a number around 60 satellite galaxies, the corresponding number for a CDM-only case would be ∼160. A suppression of the matter perturbations at small scales (as, for instance, that associated to a noncold dark matter component) is required, in order to match the predicted number and the observed one.

---

[7]For pioneer work on WDM cosmologies see Refs. [67–71].

We can also note from the two panels of Fig. 3 that the allowed contours in the (S_8, T_X/T_ν) and (S_8, f_X) planes after considering the MW dwarf satellite galaxies likelihood do not deviate significantly from the CMB constraints. This shows that the second dark matter component required to fully explain the satellites counts at galactic scale does not help in solving the tension in the S_8 parameter that exists between Planck CMB and KiDS weak lensing data. On the other hand, there exists also the possibility that the current measures of the number of MW dwarf galaxies are only underestimations of the true number, and future observations will increase the present statistics. Figure 3 illustrates also such a possibility, when combining MW satellite number counts with CMB data. In this more conservative approach to the MW satellites problem, we can notice that the satellites limits on f_X overlap with those from the CMB, adding no extra information on the noncold dark matter abundance.

Finally, the fourth panel of Fig. 4 shows the one-dimensional posterior distribution of the Hubble constant H_0. Notice that, as in the case of Ref. [21] for other possible extensions of the ΛCDM scheme, the Hubble parameter values show a better agreement with direct estimates of H_0 [77,78] in the MDM scheme than in the pure cold dark matter scenario. The Planck constraint on the Hubble constant in the MDM scenario explored here ($H_0 = 68.5 \pm 0.9$ km s^{-1} Mpc^{-1}) is higher than in the pure ΛCDM case ($H_0 = 67.3 \pm 1$ km s^{-1} Mpc^{-1}), i.e. the mean value of H_0 is shifted by approximately 1.5σ. The reason for the larger preferred value of H_0 in the context of MDM scenarios can be understood as follows. From Fig. 2 it is straightforward to infer that the value of Ω_m in these scenarios is generically lower than in the pure ΛCDM case. This fact is reinforced when combining Planck and KiDS data. As the CMB peaks structure does not leave much freedom on the value of the physical (total) matter energy density $\Omega_m h^2$, a smaller value of Ω_m requires the mean value of H_0 to be larger, in order to leave the product $\Omega_m h^2$ unchanged. When combining Planck CMB and KiDS data sets we obtain $H_0 = 70.0 \pm 0.6$ km s^{-1} Mpc^{-1}, showing a much better matching to the Hubble parameter value extracted from local observations. This value, for instance, is consistent (within 1σ) with that of Ref. [77], $H_0 = 72.5 \pm 2.5$ km s^{-1} Mpc^{-1}, and the 3.4σ tension within the ΛCDM paradigm between CMB and the Hubble constant estimates of Ref. [78], $H_0 = 73.24 \pm 1.74$ km s^{-1} Mpc^{-1}, is reduced to the 2σ level. Finally, the combination of MW satellites and Planck data leaves unchanged the value of H_0 from CMB alone in MDM scenarios, as expected, since MW satellites observations do not require a change on the dark matter abundance but on its nature, and therefore no shift is required in H_0.

IV. CONCLUSIONS

Observations at galactic and subgalactic scales compromise the viability of the canonical ΛCDM paradigm, which otherwise provides an excellent fit to large scale structure and cosmic microwave background (CMB) observations. The number of satellite galaxies in Milky-Way (MW) sized halos and the measured kinematics of the MW satellites pose the question of whether a universe made out of a pure cold dark matter component and a dark energy fluid can successfully explain all cosmological observations. Furthermore, there are a number of additional inconsistencies among small scale predictions from the ΛCDM model and observations from recent data releases from tomographic weak gravitational lensing surveys, as those from the Kilo Degree-450 deg^2 Survey (KiDS-450) [20,21]. More concretely, there are discrepancies in the value of the amplitude of the density fluctuations at a given matter density Ω_m, commonly quantified in terms of $S_8 = \sigma_8 \sqrt{\Omega_m}$.

Models with an admixture of cold and noncold dark matter particles (MDM models) may potentially alleviate the ΛCDM observational problems outlined above, as the free streaming nature associated to a nontotally cold dark matter component will suppress the matter power spectrum on the smallest scales, leading to a better agreement among large and galactic and subgalactic scales measurements. Here we have analyzed these MDM scenarios using the most recent tomographic weak lensing measurements from the KiDS-450 survey, combining them with Planck CMB data. We have also studied the constraints derived using the current estimates for the observed number of MW satellite galaxies.

In a similar way to other extended cosmological models [21], the tension in the measurements from Planck and KiDS of the S_8 quantity is reduced from $2.3 - 2.8\sigma$ to 1σ in MDM scenarios. Furthermore, the value of the Hubble parameter H_0 is perfectly consistent with that measured by late universe observations [77]. We find $H_0 = 70.0 \pm 0.6$ km s^{-1} Mpc^{-1} after combining Planck CMB and KiDS tomographic weak lensing data, value which is in a good agreement with the Hubble parameter value extracted from local observations, see e.g. Ref. [77], which quotes a value of $H_0 = 72.5 \pm 2.5$ km s^{-1} Mpc^{-1}.

We have also searched for the allowed ranges on the noncold dark matter properties, as its temperature and its mass. We find a 95% C.L. upper limit $T_X/T_\nu < 0.6$ after combining Planck CMB and KiDS data. Current estimates of the number of satellite galaxies, $N_{\rm sat}^{\rm obs} = 58 \pm 11$, when translated into a standard Gaussian likelihood and combined with CMB measurements, prefer smaller values of the temperatures ratio ($0.15 < T_X/T_\nu < 0.17$ at 95% C.L.), as they would require larger values of m_X to suppress the growth of structure at the scales involved in MW halo observations. However, if current MW satellite observations are conservatively interpreted as a half-Gaussian likelihood, imposing the current measured number only as a lower limit, the lower bound on the noncold dark matter temperature disappears, and we obtain $T_X/T_\nu < 0.19$ at 95% C.L. Concerning the noncold dark matter mass

and its abundance, after combining Planck CMB and KiDS measurements, we find a (mild) preference for a sub-keV noncold dark matter particle mass, with no particular evidence for a nonzero abundance of such a component. However, satellite counts data, in their more aggressive interpretation and combined with CMB measurements, isolate the preferred regions $0.95 \text{ keV} < m_X < 2.9 \text{ keV}$ and $f_X > 0.34$ at 95% C.L., robustly establishing the need for the existence of such a keV warm dark matter particle. In the most conservative approach there is not such a preference for $f_X \neq 0$ and only a lower bound on the noncold dark matter mass exists, $m_X > 0.08 \text{ keV}$ at 95% C.L.

Therefore, a subdominant, noncold dark matter component with $m_X \sim \text{keV}$ could in principle alleviate some existing tensions between CMB and low redshift observations. However, the masses and temperatures required to explain weak lensing and MW observations are rather different. While the scale of the power spectrum suppression required by KiDS data needs a sub-keV noncold dark matter mass and a temperature $T_X \sim T_\nu/2$, the ones required by Milky Way satellites observations are associated to larger masses and smaller temperatures. Future weak lensing and MW satellites observations will further sharpen the preferred regions, either enlarging or diminishing the existing differences among the current weak lensing and MW preferred constraints for the noncold dark matter temperature and mass. Future work with simulated data will be devoted elsewhere to further corner MDM scenarios.

ACKNOWLEDGMENTS

[1] P. A. R. Ade *et al.* (Planck Collaboration), Astron. Astrophys. **594,** A13 (2016).

[2] G. Bertone, D. Hooper, and J. Silk, Phys. Rep. **405,** 279 (2005).

[3] L. Bergstrom, Ann. Phys. (Amsterdam) **524,** 479 (2012).

[4] A. Kusenko and L. J. Rosenberg, arXiv:1310.8642.

[5] A. A. Klypin, A. V. Kravtsov, O. Valenzuela, and F. Prada, Astrophys. J. **522,** 82 (1999).

[6] B. Moore, S. Ghigna, F. Governato, G. Lake, T. R. Quinn, J. Stadel, and P. Tozzi, Astrophys. J. **524,** L19 (1999).

[7] M. Boylan-Kolchin, J. S. Bullock, and M. Kaplinghat, Mon. Not. R. Astron. Soc. **422,** 1203 (2012).

[8] L. Wang, V. Gonzalez-Perez, L. Xie, A. P. Cooper, C. S. Frenk, L. Gao, W. A. Hellwing, J. Helly, M. R. Lovell, and L. Jiang, Mon. Not. R. Astron. Soc. **468,** 4579 (2017).

[9] M. R. Lovell, V. Gonzalez-Perez, S. Bose, A. Boyarsky, S. Cole, C. S. Frenk, and O. Ruchayskiy, Mon. Not. R. Astron. Soc. **468,** 2836 (2017).

[10] T. Sawala, C. S. Frenk, R. A. Crain, A. Jenkins, J. Schaye, T. Theuns, and J. Zavala, Mon. Not. R. Astron. Soc. **431,** 1366 (2013).

[11] T. Sawala *et al.*, Mon. Not. R. Astron. Soc. **457,** 1931 (2016).

[12] A. Fattahi, J. F. Navarro, T. Sawala, C. S. Frenk, L. V. Sales, K. Oman, M. Schaller, and J. Wang, arXiv:1607.06479.

[13] E. Polisensky and M. Ricotti, Mon. Not. R. Astron. Soc. **437,** 2922 (2014).

[14] M. Vogelsberger, J. Zavala, and A. Loeb, Mon. Not. R. Astron. Soc. **423,** 3740 (2012).

[15] J. A. Schewtschenko, C. M. Baugh, R. J. Wilkinson, C. Boehm, S. Pascoli, and T. Sawala, Mon. Not. R. Astron. Soc. **461,** 2282 (2016).

[16] M. R. Lovell, V. Eke, C. S. Frenk, L. Gao, A. Jenkins, T. Theuns, J. Wang, D. M. White, A. Boyarsky, and O. Ruchayskiy, Mon. Not. R. Astron. Soc. **420,** 2318 (2012).

[17] M. R. Lovell, C. S. Frenk, V. R. Eke, A. Jenkins, L. Gao, and T. Theuns, Mon. Not. R. Astron. Soc. **439,** 300 (2014).

[18] M. R. Lovell, S. Bose, A. Boyarsky, S. Cole, C. S. Frenk, V. Gonzalez-Perez, R. Kennedy, O. Ruchayskiy, and A. Smith, Mon. Not. R. Astron. Soc. **461,** 60 (2016).

[19] T. Nakama, J. Chluba, and M. Kamionkowski, Phys. Rev. D **95,** 121302 (2017).

[20] H. Hildebrandt *et al.*, Mon. Not. R. Astron. Soc. **465,** 1454 (2017).

[21] S. Joudaki *et al.*, arXiv:1610.04606 [Mon. Not. R. Astron. Soc. (to be published)].

[22] N. Aghanim *et al.* (Planck Collaboration), Astron. Astrophys. **594,** A11 (2016).

[23] M. Kilbinger *et al.*, Mon. Not. R. Astron. Soc. **430,** 2200 (2013).

[24] C. Heymans *et al.*, Mon. Not. R. Astron. Soc. **432**, 2433 (2013).
[25] P. Lemos, A. Challinor, and G. Efstathiou, J. Cosmol. Astropart. Phys. 05 (2017) 014.
[26] M. Kilbinger *et al.*, arXiv:1702.05301.
[27] T. D. Kitching, J. Alsing, A. F. Heavens, R. Jimenez, J. D. McEwen, and L. Verde, Mon. Not. R. Astron. Soc. **469**, 2737 (2017).
[28] A. Palazzo, D. Cumberbatch, A. Slosar, and J. Silk, Phys. Rev. D **76**, 103511 (2007).
[29] A. Boyarsky, J. Lesgourgues, O. Ruchayskiy, and M. Viel, J. Cosmol. Astropart. Phys. 05 (2009) 012.
[30] A. V. Maccio, O. Ruchayskiy, A. Boyarsky, and J. C. Munoz-Cuartas, Mon. Not. R. Astron. Soc. **428**, 882 (2013).
[31] D. Anderhalden, J. Diemand, G. Bertone, A. V. Maccio, and A. Schneider, J. Cosmol. Astropart. Phys. 10 (2012) 047.
[32] D. Anderhalden, A. Schneider, A. V. Maccio, J. Diemand, and G. Bertone, J. Cosmol. Astropart. Phys. 03 (2013) 014.
[33] R. Diamanti, S. Ando, S. Gariazzo, O. Mena, and C. Weniger, J. Cosmol. Astropart. Phys. 06 (2017) 008.
[34] D. H. Weinberg, J. S. Bullock, F. Governato, R. Kuzio de Naray, and A. H. G. Peter, Proc. Natl. Acad. Sci. U.S.A. **112**, 12249 (2015).
[35] Y. Ali-Haimoud and S. Bird, Mon. Not. R. Astron. Soc. **428**, 3375 (2013).
[36] U. Seljak, Mon. Not. R. Astron. Soc. **318**, 203 (2000).
[37] J. A. Peacock and R. E. Smith, Mon. Not. R. Astron. Soc. **318**, 1144 (2000).
[38] C.-P. Ma and J. N. Fry, Astrophys. J. **543**, 503 (2000).
[39] A. Cooray and R. K. Sheth, Phys. Rep. **372**, 1 (2002).
[40] A. Mead, J. Peacock, C. Heymans, S. Joudaki, and A. Heavens, Mon. Not. R. Astron. Soc. **454**, 1958 (2015).
[41] R. Takahashi, M. Sato, T. Nishimichi, A. Taruya, and M. Oguri, Astrophys. J. **761**, 152 (2012).
[42] A. Kamada, K. T. Inoue, and T. Takahashi, Phys. Rev. D **94**, 023522 (2016).
[43] R. Takahashi and K. T. Inoue, Mon. Not. R. Astron. Soc. **440**, 870 (2014).
[44] K. T. Inoue, R. Takahashi, T. Takahashi, and T. Ishiyama, Mon. Not. R. Astron. Soc. **448**, 2704 (2015).
[45] K. Kuijken *et al.*, Mon. Not. R. Astron. Soc. **454**, 3500 (2015).
[46] I. F. Conti, R. Herbonnet, H. Hoekstra, J. Merten, L. Miller, and M. Viola, Mon. Not. R. Astron. Soc. **467**, 1627 (2017).
[47] T. D. Kitching, L. Verde, A. F. Heavens, and R. Jimenez, Mon. Not. R. Astron. Soc. **459**, 971 (2016).
[48] S. Joudaki *et al.*, Mon. Not. R. Astron. Soc. **465**, 2033 (2017).
[49] A. Schneider, J. Cosmol. Astropart. Phys. 04 (2016) 059.
[50] E. Polisensky and M. Ricotti, Phys. Rev. D **83**, 043506 (2011).
[51] J. Wolf, G. D. Martinez, J. S. Bullock, M. Kaplinghat, M. Geha, R. R. Muñoz, J. D. Simon, and F. F. Avedo, Mon. Not. R. Astron. Soc., **406**, 1220 (2010).
[52] K. Bechtol *et al.* (DES Collaboration), Astrophys. J. **807**, 50 (2015).
[53] A. Drlica-Wagner *et al.* (DES Collaboration), Astrophys. J. **813**, 109 (2015).
[54] M. Boylan-Kolchin, V. Springel, S. D. M. White, and A. Jenkins, Mon. Not. R. Astron. Soc. **406**, 896 (2010).
[55] E. J. Tollerud, J. S. Bullock, L. E. Strigari, and B. Willman, Astrophys. J. **688**, 277 (2008).
[56] A. M. Brooks and A. Zolotov, Astrophys. J. **786**, 87 (2014).
[57] A. Schneider, Mon. Not. R. Astron. Soc. **451**, 3117 (2015).
[58] Q. Guo, S. White, C. Li, and M. Boylan-Kolchin, Mon. Not. R. Astron. Soc. **404**, 1111 (2010).
[59] V. Springel, J. Wang, M. Vogelsberger, A. Ludlow, A. Jenkins, A. Helmi, J. F. Navarro, C. S. Frenk, and S. D. M. White, Mon. Not. R. Astron. Soc. **391**, 1685 (2008).
[60] W. H. Press and P. Schechter, Astrophys. J. **187**, 425 (1974).
[61] G. Mangano, G. Miele, S. Pastor, T. Pinto, O. Pisanti, and P. D. Serpico, Nucl. Phys. **B729**, 221 (2005).
[62] P. F. de Salas and S. Pastor, J. Cosmol. Astropart. Phys. 07 (2016) 051.
[63] B. Audren, J. Lesgourgues, K. Benabed, and S. Prunet, J. Cosmol. Astropart. Phys. 02 (2013) 001.
[64] J. Lesgourgues, arXiv:1104.2932.
[65] A. Lewis, A. Challinor, and A. Lasenby, Astrophys. J. **538**, 473 (2000).
[66] A. Lewis and S. Bridle, Phys. Rev. D **66**, 103511 (2002).
[67] B. Moore, T. R. Quinn, F. Governato, J. Stadel, and G. Lake, Mon. Not. R. Astron. Soc. **310**, 1147 (1999).
[68] P. Bode, J. P. Ostriker, and N. Turok, Astrophys. J. **556**, 93 (2001).
[69] V. Avila-Reese, P. Colin, O. Valenzuela, E. D'Onghia, and C. Firmani, Astrophys. J. **559**, 516 (2001),.
[70] V. K. Narayanan, D. N. Spergel, R. Dave, and C.-P. Ma, Astrophys. J. **543**, L103 (2000).
[71] M. Viel, J. Lesgourgues, M. G. Haehnelt, S. Matarrese, and A. Riotto, Phys. Rev. D **71**, 063534 (2005).
[72] M. Viel, G. D. Becker, J. S. Bolton, and M. G. Haehnelt, Phys. Rev. D **88**, 043502 (2013).
[73] J. Baur, N. Palanque-Delabrouille, C. Yeche, C. Magneville, and M. Viel, J. Cosmol. Astropart. Phys. 08 (2016) 012.
[74] V. Irsic *et al.*, Phys. Rev. Lett. **96**, 023522 (2017).
[75] C. Yeche, N. Palanque-Delabrouille, J. Baur, and H. d. M. d. BourBoux, J. Cosmol. Astropart. Phys. 06 (2017) 047.
[76] L. Lopez-Honorez, O. Mena, S. Palomares-Ruiz, and P. V. Domingo, arXiv:1703.02302.
[77] G. Efstathiou, Mon. Not. R. Astron. Soc. **440**, 1138 (2014).
[78] A. G. Riess *et al.*, Astrophys. J. **826**, 56 (2016).